JACS
JOURNAL OF THE AMERICAN CHEMICAL SOCIETY
Communication
pubs.acs.org/JACS

EMM-23: A Stable High-Silica Multidimensional Zeolite with Extra-Large Trilobe-Shaped Channels

Tom Willhammar,[†,§] Allen W. Burton,*[,‡,§] Yifeng Yun,[†] Junliang Sun,[†] Mobae Afeworki,[‡] Karl G. Strohmaier,[‡] Hilda Vroman,[‡] and Xiaodong Zou*[,†]

[†]Inorganic and Structural Chemistry and Berzelii Center EXSELENT on Porous Materials, Department of Materials and Environmental Chemistry, Stockholm University, Stockholm SE-106 91 Sweden

[‡]Corporate Strategic Research, ExxonMobil Research & Engineering Co. Inc., 1545 Route 22 East, Annandale, New Jersey 08801, United States

Supporting Information

ABSTRACT: Stable, multidimensional, and extra-large pore zeolites are desirable by industry for catalysis and separation of bulky molecules. Here we report EMM-23, the first stable, three-dimensional extra-large pore aluminosilicate zeolite. The structure of EMM-23 was determined from submicron-sized crystals by combining electron crystallography, solid-state nuclear magnetic resonance (NMR), and powder X-ray diffraction. The framework contains highly unusual trilobe-shaped pores that are bound by 21−24 tetrahedral atoms. These extra-large pores are intersected perpendicularly by a two-dimensional 10-ring channel system. Unlike most ideal zeolite frameworks that have tetrahedral sites with four next-nearest tetrahedral neighbors (Q^4 species), this unusual zeolite possesses a high density of Q^2 and Q^3 silicon species. It is the first zeolite prepared directly with Q^2 species that are intrinsic to the framework. EMM-23 is stable after calcination at 540 °C. The formation of this highly interrupted structure is facilitated by the high density of extra framework positive charge introduced by the dicationic structure directing agent.

Zeolites have shown vast applications in catalysis, sorption, separation, and ion exchange because of their unique pore size and shape selectivity. High-silica aluminosilicates with three-dimensional (3D) intersecting channels are especially interesting as selective heterogeneous catalysts in petrochemical and fine chemical industry due to their high hydrothermal stabilities. There is continuing interest in preparing zeolites with extra-large pores defined by 14 or more tetrahedral T atoms because of their potential to process larger molecules. Preparations of silicate-based molecular sieves with extra-large pores have been known since 1995, when the 14-ring zeolite UTD-1 was first reported.[1] Since that time researchers have discovered other one-dimensional 14-ring zeolites, including CIT-5,[2] SSZ-53,[3] and SSZ-59.[3] Although these zeolites have extra-large pores, their one-dimensional nature still imposes diffusional barriers and size constraints on possible transition states in bimolecular reactions. In 2003, the structure of ECR-34, a gallosilicate (Si/Ga = 3) with 18-ring pores was reported.[4] Unfortunately, the tunability of its acidic properties is limited both by its hydrothermal stability and by the narrow range of Si/Ga ratios over which it can be prepared. Later, a number of extra-large pore zeolites containing multidimensional channels were reported in germanosilicates, such as IM-12[5a]/ITQ-15[5b] (14 × 12 × 12), ITQ-37[6] (3D, 30-ring), ITQ-43[7] (28 × 12 × 12), ITQ-33[8] (18 × 10 × 10), ITQ-40[9] (16 × 15 × 15), and ITQ-44[10] (18 × 12 × 12). These zeolites contain a double four-ring (D4R) subunit, a ubiquitous feature in zeolites containing a high concentration of germanium.[11]

Although the inclusion of germanium has led to many desirable frameworks, it presents practical limitations on the preparation of commercially viable catalysts. One hurdle is that germanium is relatively rare and expensive. Furthermore, zeolites with high concentrations of framework germanium tend to be hydrolytically unstable. Once calcined to remove the organic structure directing agents (OSDAs), the zeolite framework collapses when exposed to humid air. This presents a major obstacle in any large-scale handling of the catalyst. Thus, it is highly desirable to prepare open zeolites with extra-large pores without using rare elements that either are prohibitively expensive or do not produce a sufficiently stable catalyst. Herein we present the synthesis and structure of the first stable, high-silica aluminosilicate zeolite EMM-23, with 3D channels and extra-large 21−24-ring pores.

EMM-23 was discovered from preparations in gels with Si/Al > 50 using either 1,1-(pentane-1,5-diyl)bis(1-propylpyrrolidinium) hydroxide or 1,1-(hexane-1,6-diyl)bis(1-propylpyrrolidinium) hydroxide as the OSDA (Figure S1).[12] The gels differ from typical hydroxide-mediated preparations in that they contain small concentrations of water (H_2O/Si = 4−10), and no alkali cations were used. Higher water contents lead to the formation of ZSM-5. The powder X-ray diffraction (PXRD) pattern (Figure S2) can be indexed in a hexagonal unit cell with a = 19.875(2) and c = 13.910(1) Å. The hexagonal symmetry is readily apparent in the highly faceted crystal morphologies (Figure S3). The systematic absences narrowed the likely space groups to $P6_3mc$, $P\text{-}62c$, $P6_3/mmc$, $P31c$, and $P\text{-}31c$. After calcination in air at 540 °C, the unit cell dimensions shorten to 19.629(3) and 13.202(3) Å (Figure S2). The zeolite can be made with Si/Al > 50, as confirmed by ^{27}Al MAS NMR (Figure S4). From thermogravimetric measurements, we estimate that

Received: July 30, 2014
Published: September 8, 2014

   dx.doi.org/10.1021/ja507615b | J. Am. Chem. Soc. 2014, 136, 13570−13573

the OSDA and water comprise 24 wt % of the as-made product. This is an unusually large OSDA content for all-silica zeolites prepared in hydroxide media. Cross-polarization, magic angle spinning (CPMAS) ^{13}C NMR spectrum of the as-made EMM-23 (Figure S5) shows peak positions that are consistent with those measured for the parent OSDA molecule, suggesting that the molecule is occluded intact within the zeolite structure. The calcined product of EMM-23 shows steep uptake rates for *n*-hexane (0.12 g/g), 2,2-dimethylbutane (0.073 g/g), and 2,3-dimethylbutane (0.075 g/g). The micropore volume determined from nitrogen physisorption is 0.28 cm^3/g, which is very high for an all-silica zeolite prepared from hydroxide-mediated syntheses. Collectively, these data indicate that EMM-23 has large or extra-large pores.

In typical all-silica zeolites made from hydroxide-mediated gels with positively charged OSDA molecules, there must be defects in the ideal SiO_2 framework to create a negative charge within the silica framework. These defect "nests" are created by breaking two Si−O−Si bonds to produce one siloxy (Si−O^-) and three silanol (Si−OH) species per extra framework positive charge.[13] The resultant silanol and siloxy species are referred to as "Q^3" silicon because they possess three next nearest silicon atoms in their connectivity. During calcination to remove positively charged organocations, most of the broken bonds condense (Si−OH + Si−OH → Si−O−Si + H_2O) to create Q^4 species. An alternative possibility is a silicate framework that possesses an interrupted structure with crystallographically ordered silanol and siloxy species that compensate the charge of the occluded organocations. This has been observed in the high-silica zeolite SSZ-74,[14] which has an interrupted structure with ordered Q^3 species.[15] From these considerations, we speculated that EMM-23 might also possess ordered siloxy and silanol groups.

^{29}Si MAS NMR of an all-silica, as-made sample of EMM-23 shows that there are at least five different resolvable components in the spectrum (Figure S6). The one major and two minor components between −105 and −118 ppm correspond to Q^4 silicon species and represent 67% of the total ^{29}Si signal intensity. The peaks at −88.1 and −98.4 ppm, which are assigned to Q^2 and Q^3 Si species, account for 7% and 26% of the total ^{29}Si signal intensity, respectively. These observations indicate that the structure of EMM-23 is highly interrupted. This is also the first time that Q^2 species have been observed in a zeolite *without* post-synthesis modification.

The polycrystalline nature, the large unit cell, and especially the presence of Q^2 and Q^3 Si species make the structure determination of EMM-23 challenging. Electron crystallography has unique advantages for structure solution of nano- or micron-sized crystals, which are too small to be studied by single crystal X-ray diffraction or too complex to be studied by PXRD.[16] The crystallographic phase information from high-resolution transmission electron microscopy (HRTEM) images has been used to facilitate the structure solution from PXRD data of complex zeolites, e.g., TNU-9[17] and IM-5.[18] HRTEM images from different projections were combined to obtain 3D structures of the ITQ-39 zeolite family.[19] Recently we developed the rotation electron diffraction (RED) method for collection and processing of 3D electron diffraction data.[20] A number of zeolite structures were solved from the RED data.[11h,21,22]

In order to determine the symmetry of EMM-23, we collected HRTEM images along the *c*- and *a*-axis (Figure 1a,b). Extra-large triangular-shaped channels can be seen in the HRTEM image along the *c*-axis (Figure 1a), while smaller channels can be seen in the HRTEM image along the *a*-axis (Figure 1b). The plane group was determined to be *p*31*m* along *c* and either *pmg* or *pg* along *a*. This gives two possible space groups for EMM-23: *P*-62*c* or *P*31*c*.

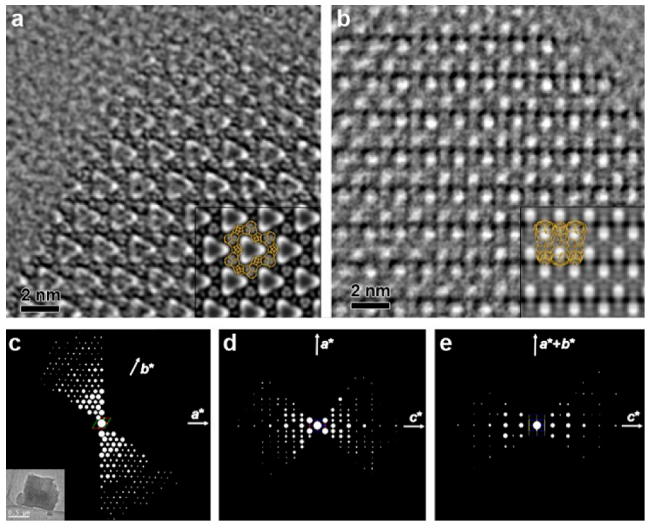

Figure 1. (a,b) Reconstructed HRTEM images of as-made EMM-23 taken along the (a) *c*- and (b) *a*-axes. The projected potential maps with (a) *p*31*m* and (b) *pmg* symmetry are inserted together with the structure model. The extra-large channels and 5-rings are clearly seen in (a). The 10-ring channels can also been recognized in (b). (c−e) 2D slices of the reconstructed 3D reciprocal lattices obtained from the RED data.

In order to solve the structure of EMM-23, 3D RED data consisting of 252 ED fames covering a tilt range of 63.74° were collected (see Table S1). The advantages of RED compared to HRTEM are that higher resolution and more complete data can be obtained from the same crystal, due to the lower electron dose needed for electron diffraction. Figure 1c−e shows the two-dimensional (2D) slices cut from the 3D reciprocal lattice reconstructed from the RED data. The reflection conditions were deduced as *hhl*:*l* = 2n and 00*l*:*l* = 2n. A few reflections in Figure 1e violate the reflection conditions due to double diffraction. The original RED data and reconstructed 3D reciprocal lattice are shown in Movies S1 and S2, respectively.

The structure model of EMM-23 was obtained from the RED data by direct methods based on the space group *P*-62*c*. It contains eight four-connected T-sites and one three-coordinated T-site. The crystal data and refinement results are given in Table S1. The structure model is in good agreement with the HRTEM images, see Figure 1a,b. In the view of the model along the [1-10] direction it can be seen that one of these T atoms (circled in blue in Figure S7b) is prohibitively close to a symmetry-equivalent position. Clearly, this site can only be partially occupied. The site cannot be merged onto the high symmetry position without creating unfavorable bond lengths with the neighboring oxygen atoms. Depending upon which symmetry-equivalent site is removed, the silicon site between each pair (circled in yellow in Figure S7a−d) may be either a Q^2 or Q^3 species.

The structure model obtained from HRTEM and RED was further refined against synchrotron PXRD data of both an as-made sample and an OSDA-free sample obtained by treating with ozone at 150 °C. During the refinement it was clear that in order to obtain a proper geometry of the framework, a lower

dx.doi.org/10.1021/ja507615b | J. Am. Chem. Soc. 2014, 136, 13570−13573

symmetry space group $P31c$ has to be chosen (Figure S7e). Because the PXRD data of the as-made EMM-23 show the highest quality in terms of resolution and peak shape, we present the results of its refinement here. The results of Rietveld refinement of the ozone-treated sample are given in the Supporting Information (Figure S8). The final agreement factors for the Rietveld refinement of the as-made material are Rwp = 10.2%, Rp = 7.6%, and χ^2 = 2.41. The two T-sites that occupy the "cusps" of the trilobe have partial occupancies of 0.67 and 0.33. The Q^4:Q^3:Q^2 ratio in the structure depends on the occupancy of these two sites. The total ratios can be calculated statistically from four different models produced by altering the presence of the two sites and weighting the occupancies achieved from the Rietveld refinement. The ratio calculated from the refined model is 72:23:5 for Q^4:Q^3:Q^2, which is in good agreement with the results from ^{29}Si MAS NMR of 67:26:7 for Q^4:Q^3:Q^2, respectively. The Rietveld plots in Figure 2 show excellent agreement between the simulated and experimental profiles.

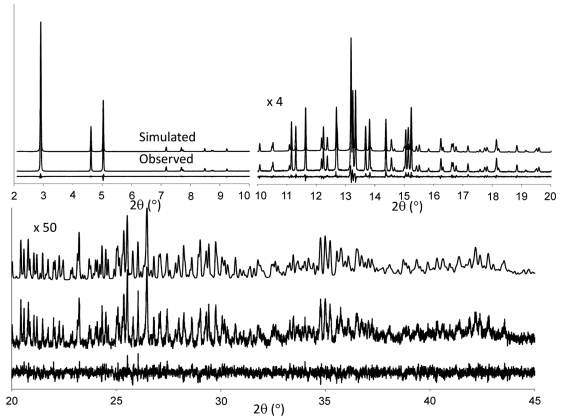

Figure 2. Simulated (top), observed (middle), and difference (bottom) profiles for the Rietveld refinement of as-made EMM-23 (λ = 0.8668 Å).

The final refined structure of EMM-23 in $P31c$ contains 13 symmetry-independent Si atoms, out of which two are partially occupied (Si4 and Si11, with the occupancy of 1/3 and 2/3, respectively). The structure is built from a $[5^77^1]$ unit containing 17 fully occupied SiO_4 tetrahedra and two partially occupied SiO_4 tetrahedra (Figure 3a). The $[5^77^1]$ units are connected by sharing four tetrahedra to form a chain along the c-axis (Figure 3b). The neighboring $[5^77^1]$ units in the chain are related by a c-glide in the ac or bc plane (Figure 3c). The chains, which are related to one another by 3-fold axes, are connected by sharing four tetrahedra to form a 3D framework (Figure 3d). The framework formed by the fully occupied tetrahedra contains 24-ring channels along the c-axis, which intersect with zigzag 10-ring channels perpendicular to the c-axis to form a 3D channel system (Figure 3e, Movie S3). The presence of the partially occupied terminal tetrahedra, however, reduces the size of the 24-ring channels. With the full occupation of the terminal tetrahedra, the 24-ring channel is reduced to 21-ring. The average ring size of the final refined structure is 22. The dimensions of the 10-ring channels are not affected by the partially occupied tetrahedral atoms since none of these sites are contained within the 10-ring window. The decrease of the c-parameter after calcination is probably due to condensation of some terminal tetrahedra.

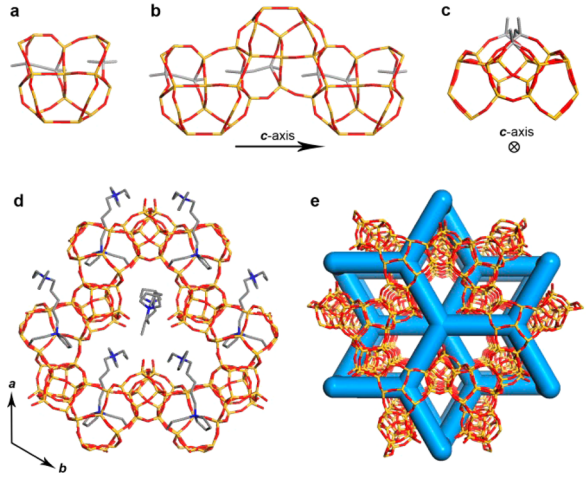

Figure 3. Construction of the 3D framework of EMM-23. (a) The $[5^77^1]$ building unit with two partially occupied and three-connected T atoms (in gray) attached. Three $[5^77^1]$ building units connected by sharing four T atoms to form a chain along the c-axis viewed along (b) the [110] direction and (c) the c-axis. (d) The 3D framework viewed along the c-axis. (e) The 3D channel system with straight channels along c-axis and interconnecting zigzag channels perpendicular to the c-axis. The channels system follows the topology of graphite, **gra**. The Si, O, C, and N atoms are in yellow, red, gray, and blue.

Figure 3d shows the two configurations of the OSDA molecule determined from the Rietveld refinement, which agree with those obtained by energy-optimization (Figure S9). It should be noted that there are water molecules close to the position of one of the OSDA molecules. The partial occupancies of the OSDA molecule and the water molecules suggest that these positions are not occupied simultaneously. The framework of EMM-23 follows the topology of the **acs** net. Each node of the **acs** net is decorated by three $[5^77^1]$ units arranged around the 3-fold axis. The topology of the channels follows the graphite-type net, **gra** (Figure 3e). The channel system is limited to a ring with a size between 21 and 24 T-sites. The framework density of the Rietveld refined model is 13.9 T/1000 Å^3. The model with all T-sites fully occupied has a framework density of 15.2 T/1000 Å^3.

Because of the irregularly shaped channels, it is difficult to assign pore sizes that assess which molecules can diffuse within the pores along the 3-fold axis. A projection of the pore with dimensions between selected pairs of O atoms (Figure S10) shows the distance between the cusp and the end of its opposing lobe is about 10 Å, while the distance between the ends of adjacent lobes is about 12 Å. The width of the lobe is particularly difficult to define because of the fractional occupancies of the oxygen sites on the cusp. The size of the entrance into the lobe from the middle of the pore also varies along the c-axis. The distances vary between 2.7 and 5.2 Å depending on which pairs of opposing oxygen atoms are chosen. The widest dimension within the lobe is about 5.2 Å. The dimensions of the 10-rings that connect the cage structures to the lobe are 5.1 × 5.4 Å.

One of the most important features of the EMM-23 framework is the unique shape selectivity that it offers. Large molecules, e.g., polyalkyl aromatics, may absorb within the centers of the extra-large channels, but only small functional groups or chains may penetrate into the lobes or 10-ring cavities. This might combine the shape selective catalysis observed in 10-ring zeolite with the possibility of introducing

dx.doi.org/10.1021/ja507615b | J. Am. Chem. Soc. 2014, 136, 13570−13573

larger species into the reaction. The unusually high density of well-defined Q^2 and Q^3 sites also make the zeolite an ideal candidate for supporting metals for shape-selective catalysis. By providing anchoring sites for metal ions or complexes during post-synthetic treatments, the silanol groups should promote the formation of highly dispersed metal species within the zeolite void space. This should make reduced metal species less susceptible to aggregation. The dimensions of the extra-large pores allow the diffusion of aqueous transition-metal complexes that otherwise are too large to fit within medium pore zeolites. Finally, the structure of EMM-23 demonstrates that it is possible to synthesize *stable* zeolites with extra-large features in the absence of expensive elements like germanium. As has previously been observed in zeolite ITQ-37[6], a high density of crystallographically unique Q^3 or Q^2 species seems to result in the formation of microporous materials with large void volumes.

■ ASSOCIATED CONTENT

Supporting Information

Detailed synthetic procedures and characterization, solid-state NMR, SEM images, HRTEM and RED data collection and structure determination, movies showing the RED data and the structure of EMM-23, and crystallographic data (CIFs). This material is available free of charge via the Internet at http://pubs.acs.org.

■ AUTHOR INFORMATION

Corresponding Authors

allen.w.burton@exxonmobil.com
xzou@mmk.su.se

Author Contributions

[§]These authors contributed equally.

Notes

The authors declare no competing financial interest.

■ ACKNOWLEDGMENTS

We thank Rich McEvoy for the SEM measurements and for assistance in the syntheses which led to the initial discovery of EMM-23. We thank Eugene Terefenko for performing experiments in the optimization of the synthesis, David Griffin for the assistance in collection of the NMR data, Michele Kleinschmidt for conducting the hydrocarbon adsorption tests, Khizera Tariq for carrying out nitrogen physisorption measurements, and Jane Cheng for discussion of uptakes of different adsorbate molecules. We thank Jose Santiesteban and Stu Soled for review and discussion of our manuscript. We greatly appreciate the strong support of ExxonMobil Research and Engineering for our efforts in zeolite synthesis and discovery. We also acknowledge financial support from the Swedish Research Council (VR), the Swedish Governmental Agency for Innovation Systems (VINNOVA), and the Knut and Alice Wallenberg Foundation (KAW) through a project grant 3DEM-NATUR and a grant for purchasing the TEMs.

■ REFERENCES

(1) (a) Balkus, K. J.; Gabrielov, A. G.; Sandler, N. *Mater. Res. Soc. Symp. Proc.* **1995**, *368*, 369. (b) Freyhardt, C. C.; Tsapatsis, M.; Lobo, R. F.; Balkus, K. J., Jr.; Davis, M. E. *Nature* **1996**, *381*, 295. (c) Lobo, R. F.; Tsapatsis, M.; Freyhardt, C. C.; Khodabandeh, S.; Wagner, P.; Chen, C. Y.; Balkus, K. J.; Zones, S. I.; Davis, M. E. *J. Am. Chem. Soc.* **1997**, *119*, 8474.

(2) Yoshikawa, M.; Wagner, P.; Lovallo, M.; Tsuji, K.; Takewaki, T.; Chen, C. Y.; Beck, L. W.; Jones, C.; Tsapatsis, M.; Zones, S. I.; Davis, M. E. *J. Phys. Chem. B* **1998**, *102*, 7139.

(3) Burton, A. W.; Elomari, S.; Chen, C. Y.; Medrud, R. C.; Chan, I. Y.; Bull, L. M.; Kibby, C.; Harris, T. V.; Zones, S. I.; Vittoratos, E. S. *Chem.—Eur. J.* **2003**, *9*, 5737.

(4) Strohmaier, K. G.; Vaughan, D. E. W. *J. Am. Chem. Soc.* **2003**, *125*, 16035.

(5) (a) Paillaud, J.-L.; Harbuzaru, B.; Patarin, J.; Bats, N. *Science* **2004**, *304*, 990. (b) Corma, A.; Díaz-Cabañas, M. J.; Rey, F.; Nicolopoulus, S.; Boulahya, K. *Chem. Commun.* **2004**, *12*, 1356−1357.

(6) Sun, J. L.; Bonneau, C.; Cantin, A.; Corma, A.; Diaz-Cabanas, M. J.; Moliner, M.; Zhang, D. L.; Li, M. R.; Zou, X. D. *Nature* **2009**, *458*, 1154.

(7) Jiang, J.; Jorda, J. L.; Yu, J. H.; Baumes, L. A.; Mugnaioli, E.; Diaz-Cabanas, M. J.; Kolb, U.; Corma, A. *Science* **2011**, *333*, 1131.

(8) Corma, A.; Diaz- Cabañas, M. J.; Jorda, J. L.; Moliner, M. *Nature* **2006**, *443*, 842.

(9) Corma, A.; Diaz-Cabanas, M. J.; Jiang, J.; Afeworki, M.; Dorset, D. L.; Soled, S. L.; Strohmaier, K. G. *Proc. Natl. Acad. Sci. U.S.A.* **2010**, *107*, 13997.

(10) Jiang, J.; Jorda, J. L.; Diaz-Cabañas, M. J.; Yu, J.; Corma, A. *Angew. Chem., Int. Ed.* **2010**, *49*, 4986.

(11) (a) Barrett, P. A.; Boix, T.; Puche, M.; Olson, D. H.; Jordan, E.; Koller, H.; Camblor, M. A. *Chem. Commun.* **2003**, *17*, 2114. (b) Corma, A.; Nararro, M. T.; Rey, F.; Rius, J.; Valencia, S. *Angew. Chem., Int. Ed.* **2001**, *40*, 2277. (c) Corma, A.; Diaz-Cabañas, M. J.; Martinez-Triguero, J.; Rey, F.; Rius, J. *Nature* **2002**, *418*, 514. (d) Corma, A.; Rey, F.; Valencia, S.; Jorda, J. L.; Rius, J. *Nat. Mater.* **2003**, *2*, 493. (e) Conradsson, T.; Dadachov, M. S.; Zou, X. D. *Microporous Mesoporous Mater.* **2000**, *41*, 183. (f) Tang, L.; Shi, L.; Bonneau, C.; Sun, J. L.; Yue, H. J.; Ojuva, A.; Lee, B. L.; Kritikos, M.; Bell, R. G.; Bacsik, Z.; Mink, J.; Zou, X. D. *Nat. Mater.* **2008**, *7*, 381. (g) Yu, Z.-B.; Han, Y.; Zhao, L.; Huang, S. L.; Zheng, Q. Y.; Lin, S. Z.; Cordova, A.; Zou, X. D.; Sun, J. L. *Chem. Mater.* **2012**, *24*, 3701. (h) Hua, W.; Chen, H.; Yu, Z.-B.; Zou, X. D.; Lin, J. H.; Sun, J. L. *Angew. Chem., Int. Ed.* **2014**, *53*, 5868.

(12) Burton, A. W.; Strohmaier, K. G.; Vroman, H. Patent Application WO/2013/019462, July 2, 2013.

(13) Koller, H.; Lobo, R. F.; Burkett, S. L.; Davis, M. E. *J. Phys. Chem.* **1995**, *99*, 12588.

(14) Zones, S. I.; Burton, A. W.; Ong, K. US Patent 7 510 697, 2009.

(15) Baerlocher, Ch.; Xie, D.; McCusker, L. B.; Hwang, S. J.; Chan, I. Y.; Ong, K.; Burton, A. W.; Zones, S. I. *Nat. Mater.* **2008**, *7*, 631.

(16) Willhammar, T.; Yun, Y. F.; Zou, X. D. *Adv. Funct. Mater.* **2014**, *24*, 182.

(17) Gramm, F.; Baerlocher, Ch.; McCusker, L. B.; Warrender, S. J.; Wright, P. A.; Han, B.; Hong, S. B.; Liu, Z.; Ohsuna, T.; Terasaki, O. *Nature* **2006**, *444*, 79.

(18) Baerlocher, Ch.; Gramm, F.; Massuger, L.; McCusker, L. B.; He, Z. B.; Hovmoller, S.; Zou, X. D. *Science* **2007**, *315*, 1113.

(19) Willhammar, T.; Sun, J. L.; Wan, W.; Oleynikov, P.; Zhang, D. L.; Zou, X. D.; Moliner, M.; Gonzalez, J.; Martinez, C.; Rey, F.; Corma, A. *Nat. Chem.* **2012**, *4*, 188.

(20) Wan, W.; Sun, J. L.; Su, J.; Hovmöller, S.; Zou, X. D. *J. Appl. Crystallogr.* **2013**, *46*, 1863.

(21) Su, J.; Kapaca, E.; Liu, L. F.; Georgieva, V.; Wan, W.; Sun, J. L.; Valtchev, V.; Hovmöller, S.; Zou, X. D. *Microporous Mesoporous Mater.* **2014**, *189*, 115.

(22) Martínez-Franco, R.; Moliner, M.; Yun, Y. F.; Sun, J. L.; Wan, W.; Zou, X. D.; Corma, A. *Proc. Natl. Acad. Sci. U. S. A.* **2013**, *110*, 3749.